Article

Anodic TiO$_2$ Nanotube Layers for Wastewater and Air Treatments: Assessment of Performance Using Sulfamethoxazole Degradation and N$_2$O Reduction

Marcel Sihor [1,2], Sridhar Gowrisankaran [1], Alexandr Martaus [2], Martin Motola [1], Gilles Mailhot [3], Marcello Brigante [3] and Olivier Monfort [1,*]

[1] Department of Inorganic Chemistry, Faculty of Natural Sciences, Comenius University Bratislava, Ilkovicova 6, Mlynska Dolina, 84215 Bratislava, Slovakia

[2] Institute of Environmental Technology, CEET, VSB-Technical University of Ostrava, 17. Listopadu 15/2172, 70800 Ostrava-Poruba, Czech Republic

[3] Institut de Chimie de Clermont-Ferrand, Université Clermont Auvergne, CNRS, Clermont Auvergne INP, F-63000 Clermont-Ferrand, France

* Correspondence: monfort1@uniba.sk; Tel.: +421-290142141

Abstract: The preparation of anodic TiO$_2$ nanotube layers has been performed using electrochemical anodization of Ti foil for 4 h at different voltages (from 0 V to 80 V). In addition, a TiO$_2$ thin layer has been also prepared using the sol–gel method. All the photocatalysts have been characterized by XRD, SEM, and DRS to investigate the crystalline phase composition, the surface morphology, and the optical properties, respectively. The performance of the photocatalyst has been assessed in versatile photocatalytic reactions including the reduction of N$_2$O gas and the oxidation of aqueous sulfamethoxazole. Due to their high specific surface area and excellent charge carriers transport, anodic TiO$_2$ nanotube layers have exhibited the highest N$_2$O conversion rate (up to 10% after 22 h) and the highest degradation extent of sulfamethoxazole (about 65% after 4 h) under UVA light. The degradation mechanism of sulfamethoxazole has been investigated by analyzing its transformation products by LC-MS and the predominant role of hydroxyl radicals has been confirmed. Finally, the efficiency of the anodic TiO$_2$ nanotube layer has been tested in real wastewater reaching up to 45% of sulfamethoxazole degradation after 4 h.

Keywords: photocatalysis; pharmaceutical; water treatment; air treatment; N$_2$O; TiO$_2$

1. Introduction

With regard to a number of publications, titania (TiO$_2$) is the most investigated photocatalyst in a multitude of applications such as, for example, antibacterial coatings and water and air treatments [1–6]. Efficient TiO$_2$ photocatalysts are prepared in the form of nanomaterials ranging from 0D to 3D morphologies [5,7–12]. The 1D titania nanostructures include TiO$_2$ nanotubes (TNT) that are promising nanostructured photocatalysts mainly due to their excellent electron transport [13–15]. In the form of self-organized arrays (i.e., supported layers), TNT exhibit enhanced charge carriers separation, thus leading to exceptional photocatalytic properties [13–16]. The preparation TNT layers can be conducted by anodic oxidation of a Ti electrode in a fluoride-containing electrolyte [17–19]. The variation in applied voltage, fluoride concentration and anodization time can be tuned to design TNT of specific length and wall thickness [17–20]. In addition, by extending one of these experimental parameters, the TNT morphology can be transformed in a porous nanostructure, which also exhibits interesting photocatalytic properties as reported in our recent study [20]. Indeed, by increasing the anodization voltage, it is possible to form a porous sponge-like structure.

The treatment of water by photocatalysis is one of the most investigated alternatives to enhance the already existing processes which are used in wastewater treatment plants

(WWTPs) and in the production of drinking water [21]. Indeed, the photocatalytic process belongs to advanced oxidation processes (AOPs), thus generating reactive oxygen species (ROS) such as hydroxyl radicals (HO•) [22]. Using a semiconductor photocatalyst such as TiO_2, UVA light is necessary to generate the electron/hole (e^-/h^+) pair, from which h^+ reacts with water to produce HO•. The HO• react with high kinetic rate and non-selectively with organic molecules including persistent organic pollutants (POPs) and contaminants of emerging concern (CECs) [22]. Among CECs, pharmaceutical and personal care products (PPCPs) are consumed daily and their long-term impact on the natural environmental and human health is not yet clarified [23,24]. Intergovernmental agencies have implemented stringent norms for pollution control and water quality, such as the implementing decision of the European Union (EU) No. 2020/1161 on the directive No. 2008/105/CE [25]. Therefore, the modification of conventional water treatments appears a necessary conditions to fulfill these norms, especially by adding or replacing current chemical oxidation processes with AOPs; thus, TNT photocatalysts are an excellent candidate. In this study, sulfamethoxazole (SMX) is used as a model pollutant since it is a widely used antibiotic. In addition, SMX is one of the most frequently detected pollutants in water around the world [23].

The treatment of air for the removal of nitrous oxide (N_2O) using photocatalytic reactions was described back in the 1990s, when the first experiments employed zeolite containing Cu-based photocatalysts [26]. N_2O is in the top 3 gases responsible for global warming, since it has been proven to be involved at 6.2% of the total global radiative forcing. The major origin of N_2O is from natural processes (nitrification of ammonia, denitrification of nitrates, etc.) but also anthropogenic activities (N-based fertilizers, combustion of fossil fuels, etc.) [27]. Therefore, intense research is being carried out to develop different types of photocatalysts including TiO_2 [28–33]. However, one significant disadvantage of these already existing photocatalysts is that they are not easy to handle because of their powder form. Using supported TNT photocatalysts, such a drawback might be overcome.

In the present study, the use of anodic TNT layers in wastewater and air treatments is assessed using the degradation of aqueous sulfamethoxazole solution and the reduction of gaseous nitrous oxide, respectively, as model reactions. To the best of our knowledge, it is the first time that anodic TiO_2 layers either in the form of nanotubal or sponge-like structure are used in such versatile photocatalytic reactions, and their performance is compared to another TiO_2 nanostructure i.e., TiO_2 thin layer deposited by the sol–gel method. Such a comparative study will bring further insights into the application of TiO_2 nanomaterials for environmental purposes. In addition, the degradation of SMX is also performed in real wastewater and the degradation pathway of SMX is proposed, so the fundamental understanding of the prepared materials is coupled with semi-applied science, which is the early stage of industrial application development.

2. Results and Discussion

2.1. Structural and Optical Properties of Photocatalysts

The XRD patterns (Figure 1) of the F20, F40, F60, F80 and SG samples match with the anatase phase of TiO_2 (ICDD card no. 03-065-5714) as reported in our previous studies [20,34]. Very weak diffractions of TiO_2 anatase phase are also confirmed in the SG sample, where a textured silicon wafer was used as the substrate. Therefore, additional diffractions of the textured silicon wafers correspond to the K_{beta}, L_{alpha1} and L_{alpha2} lines of Si (111) along with impurities. It is worth noting the diffractions from metallic Ti in the TNT layers since it is the underlying substrate of self-organized and highly oriented TiO_2 nanotubes. In addition, the F0 sample only exhibits metallic Ti diffraction (ICDD card no. 00-044-1294), although an ultra-thin layer of TiO_2 (several nanometers) might be present due to surface oxidation.
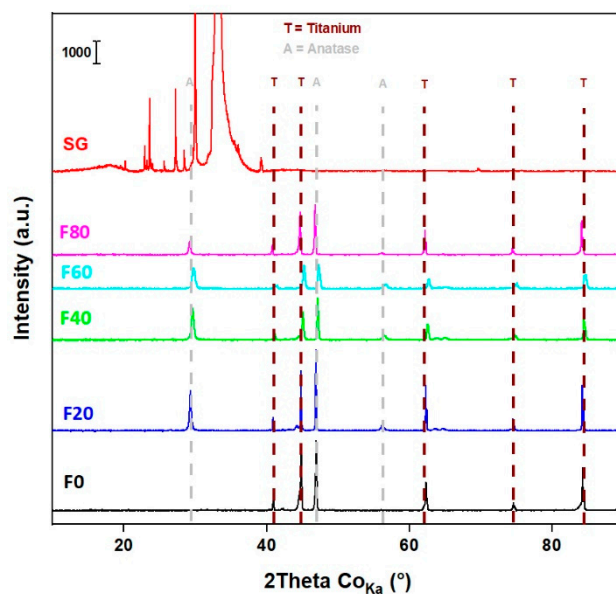
Figure 1. XRD of the TiO$_2$ nanostructures.

The surface and cross-section morphology of the samples have been characterized by SEM in previous studies [20,34,35] and comprehensively discussed. Briefly, the surface of the F0 sample exhibits the typical morphology of Ti, i.e., a dense structure of micro-crystals. As the anodization voltage increases from 20 to 80 V, a porous nanostructure is formed. The F20 sample exhibits the clear nanotubular morphology of a self-organized and highly-ordered TNT layer, while the surface of the TNT in the F40 sample starts to be destroyed. In the F60 and F80 samples, the nanotubular morphology disappears and a porous nanostructure composed of a reminiscent nanotube and a sponge-like structure is formed, respectively.

Concerning the optical properties, the Tauc's plot (Figure 2) exhibits that the samples showing TNT morphology i.e., F20 and F40, possess the strongest light absorption, along with E_g, of about 3.28 eV. For porous nanostructures such as the F60 and F80 samples, light absorption decreases while the E_g is about 3.35 eV. For the SG sample, light absorption is weaker due to the thickness, which is approx. 5 times thinner than anodized samples. In addition, the F0 sample which is essentially composed of metallic Ti exhibits slight absorption in UVA due to the upper oxidized layer.
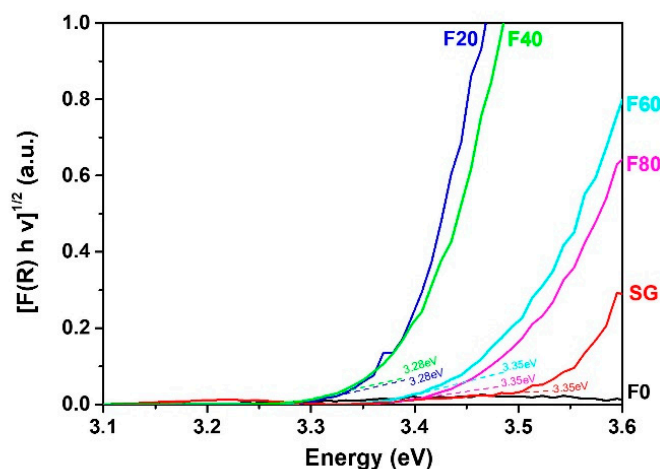

Figure 2. UV-visible DRS of the TiO$_2$ nanostructures.

2.2. Reduction of N$_2$O

The ability of the TiO$_2$ photocatalysts prepared by two different methods (electrochemical anodization and sol–gel deposition) to reduce nitrous oxide under UVA light is investigated (Figure 3). It is worth noting there is no reference in the literature about testing the photocatalytic decomposition of N$_2$O with the use of a TiO$_2$ nanostructure prepared by electrochemical anodization, thus highlighting the significance of the present study.
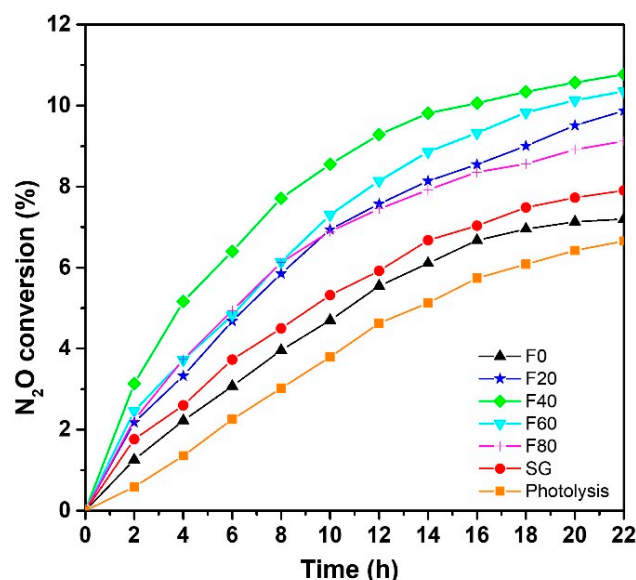

Figure 3. N$_2$O gas conversion under UVA light.

From Figure 3, it is clear that N$_2$O conversion, which occurs during photocatalytic reactions, is significantly higher than direct photolysis (i.e., without photocatalyst). Comparing the different photocatalysts, the highest N$_2$O conversion is achieved using samples prepared by electrochemical anodization, especially the F40 sample, showing nanotubular morphology. Indeed, such a TNT layer can convert about 10% of N$_2$O after 22 h UVA irradiation. The lowest photocatalytic activities are observed for F0 and SG samples with a conversion about 7.2% and 7.9%, respectively. This is due to two main reasons: (i) these samples exhibit a significantly lower specific surface area compared to nanoporous F20, F40, F60 and F80 and (ii) their thickness is also smaller. Nevertheless, both of these poorly photoactive samples present a higher N$_2$O conversion than simple photolysis (6.6%).

2.3. Degradation of SMX

The degradation curves of SMX using the samples prepared by electrochemical anodization and the sol–gel method are presented in Figure 4, along with the reusability of the best sample (F20) after 3 repeated runs (Figure S1). Globally, a similar trend is observed between N$_2$O reduction and SMX oxidation since the best samples are F20 and F40, i.e., samples with nanotubular morphology. This fact highlights the versatility of anodic TiO$_2$ nanotube layers. The degradation extent of SMX after 4 h UVA irradiation reaches 65% and 62% for in the presence of F20 and F40, respectively. The degradation extent decreases to 52% using F60, since the structure is composed of reminiscent nanotubes. The efficiency of the other samples is relatively poor due to the absence of nanotubular morphology. In other words, the number of catalytic sites and the lifetime of charge carriers is probably significantly reduced. The TOC analysis corroborates the degradation curves. Indeed, for F20, F40 and F60, the mineralization extent after 4 h UVA irradiation reaches 11%, 8% and 3%, respectively, while for the other samples, no mineralization takes place. The potential application of anodic TiO$_2$ layer in water treatment is performed by the degradation of SMX in secondary effluents of wastewater treatment plants (Figure S2). The degradation efficiency decreases from 65 to 45% due to the negative effects of the wastewater matrix,

i.e., the dissolved organic matter that plays the role of ROS scavenger. However, the degradation efficiency is still considered to be satisfactory.
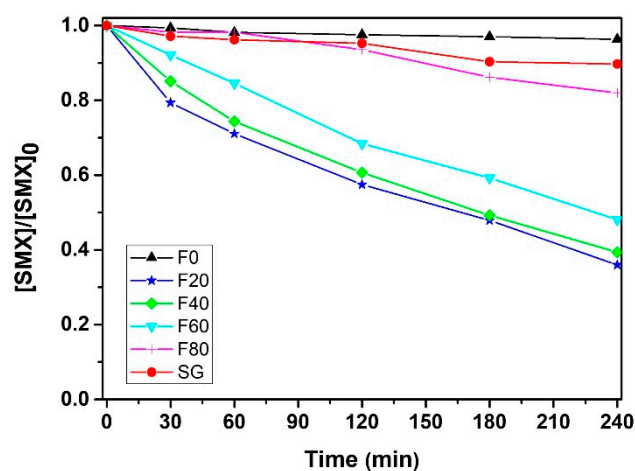

Figure 4. Degradation of SMX under UVA light.

In order to obtain better insights into the degradation mechanism using F20, the SMX degradation by-products are identified using LC-MS. The transformation products of SMX are presented in Table S1 (Supplementary Materials). The initial SMX molecule displayed a peak at $[M + H]^+ = 254.0592$ and a sodium adduct $[M + Na]^+ = 276.0410$ and $[M − H]^- = 252.0441$. Different degradation pathways are proposed considering the identification of SMX by-products (Figure 5). The formation of P1 occurs through the photo-isomerization of the isoxazole ring, which is also the dominant pathway in the degradation of SMX under UV-mediated degradation [36]. Electrophilic reaction on the aromatic ring leads to the formation of hydroxylated (P2) and dihydroxylated (P3) products, while oxidation of the double bond at the isoxazole ring produced P4. The cleavage of sulfonamide bond by the hydroxyl radical leads to the formation of 3-amino-5-methylisoxazole (P5) and sulfanilic acid (P4). Isoxazole ring rearrangement leads to the formation of P7 that can be further oxidized on the amine ring in the presence of a hydroxyl radical, leading to the formation of P7 and P8. The degradation mechanism confirms the predominant role of hydroxyl radicals.
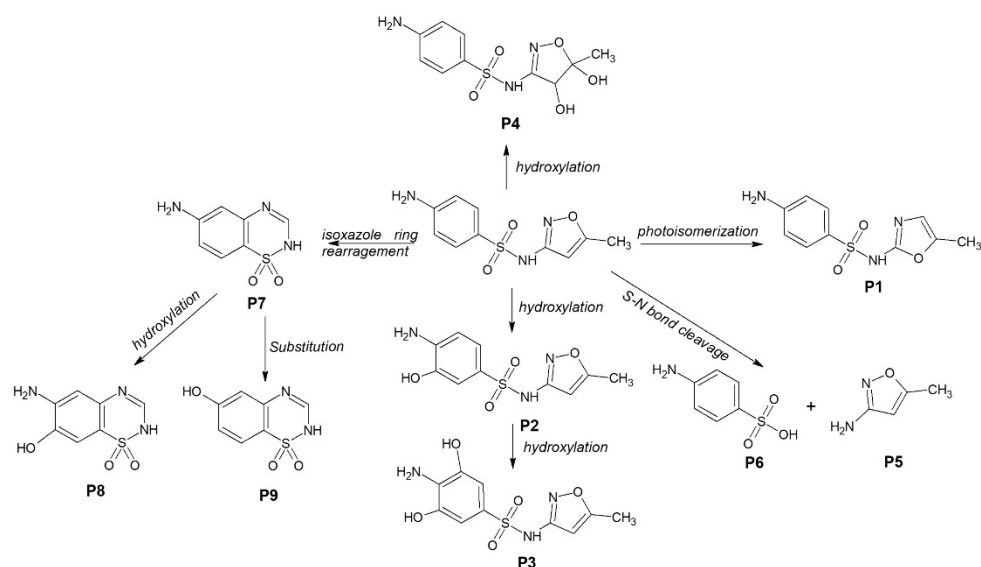

Figure 5. Proposed mechanism of SMX degradation under UVA light in the presence of anodic TiO_2 nanotube layer.

3. Materials and Methods

3.1. Preparation and Characterization of Photocatalysts

The TNT layers are prepared using a similar procedure reported in one of our previous study [34]. Briefly, a disk of 4 cm in diameter of titanium foil (Merck, Darmstadt, Germany, 99.7% with 0.127 mm thickness) is used as a working electrode and dropped in fluoride-based electrolyte based on glycerol. The counter electrode is also a 4 cm diameter Ti foil. The distance between the two electrodes is set at 1.5 cm and electrochemical anodization is performed at different applied voltages from 0 to 80 V (with a 20 V step) for 100 min. The current intensity is kept at 5 A during the procedure. After rinsing the as-prepared TNT followed by annealing at 400 °C for 1 h, TNT layers labelled F0, F20, F40, F60 and F80 are obtained.

For comparison, TiO_2 sol–gel films are prepared. To this end, titanium isopropoxide (97.0%; Merck, Darmstadt, Germany) is added to isopropanol (reagent grade, Slavus, Bratislava, Slovakia) containing acetic acid (99.0%, Slavus, Bratislava, Slovakia) and Triton® X-100 (Merck, Darmstadt, Germany) as chelating and structure directing agents, respectively, thus a 0.2 M Ti alkoxide sol–gel is obtained. The sol–gel is deposited by spin-coating (Ossila Ltd.) at 2000 rpm on Si wafer (University Wafer Inc., South Boston, MA, USA) with a diameter of 4 cm. Six-layer films are prepared with intermediate annealing at 300 °C for 10 min and final annealing at 450 °C for 1 h. The TiO_2 sol–gel films are labelled SG.

The TNT and sol–gel layers are characterized by DRS (Shimadzu UV-2600, IRS-2600 Plus) and XRD (Rigaku SmartLab) to control the optical energy band gap (E_g) and the crystalline phase composition. The optical energy band gap is determined using the Kubelka-Munk theory (Equation (1)) by assuming an indirect band gap, i.e., $z = 2$. The value of E_g is determined by the linear extrapolation of the plot with the *x*-axis. Further characterization details of these reproducible nanomaterials are provided in our previous publications [20,34,35].

$$(F(R)\, h\nu)^{1/z} = B\,(h\nu - E_g)\qquad(1)$$

where $F^®$ is the absorption spectra, h is the Planck constant, E_g is the energy band gap, z is a factor depending on the type of E_g, ν is the incident light frequency and B is a constant.

3.2. Degradation of N_2O in the Gas Phase

The photocatalytic decomposition of gaseous N_2O is performed in a custom-made stainless-steel photo-reactor (Figure 6), where the photocatalytic layer is placed at the bottom. After that, the reactor is closed and filled with a N_2O/He mixture and pressurized to 1.5 bar (pressure is controlled during the whole experiment). The initial N_2O concentration is set at 1030 ppm. The irradiation is generated by a UVA source (UVP Pen-Ray, 8 W Hg lamp; $\lambda_{max} = 365$ nm) situated at the top of a photo-reactor, through the quartz glass visor. The N_2O concentration is measured using a GC/BID (Gas Chromatography coupled with Barrier discharge Ionization detector, Shimadzu Tracera GC 2010 Plus) in two hour-intervals for 22 h. Each experiment is repeated to check the reproducibility. The conversion of N_2O (R_{N_2O}) is calculated using Equation (1), where $x^0_{N_2O}$ is the initial mole fraction of N_2O and x_{N_2O} is the mole fraction at different times during the photocatalytic reaction.

$$R_{N_2O} = \frac{x^0_{N_2O} - x_{N_2O}}{x^0_{N_2O}}\qquad(2)$$

3.3. Degradation of SMX in Water

Concerning the photocatalytic degradation of SMX solution (50 µM), the photocatalytic layers are placed at the bottom of a homemade photo-reactor equipped of four UVA lamps at the top (Sylvania F15W/350BL; 1.9 mW cm^{-2} in the range 290–400 nm). Prior to turning on the lamps, the initial pH of SMX solution is adjusted at 7 using $HClO_4$ and NaOH. The photocatalytic degradation is performed under constant air bubbling for 4 h and 500 µL is sampled out every 30 min (filtration through 0.45 µm PTFE filter and quenching into

100 μL methanol). The concentration of SMX is analyzed by HPLC (Shimadzu Nexera XR LC-20AD) equipped with a C18 column (Agilent, EC 250/4.6 nucleodur 100/5). The mobile phase is a mixture of MeOH/H_2O in gradient mode from 40:60 (*v/v*) to 95:5 (*v/v*), which is achieved in 10 min. The detection wavelength of SMX is fixed at 268 nm. It is worth noting that the degradation experiments are repeated three times to control the reusability of the photocatalytic layers and the variations in degradation efficiency do not exceed 5% (Figure S1).
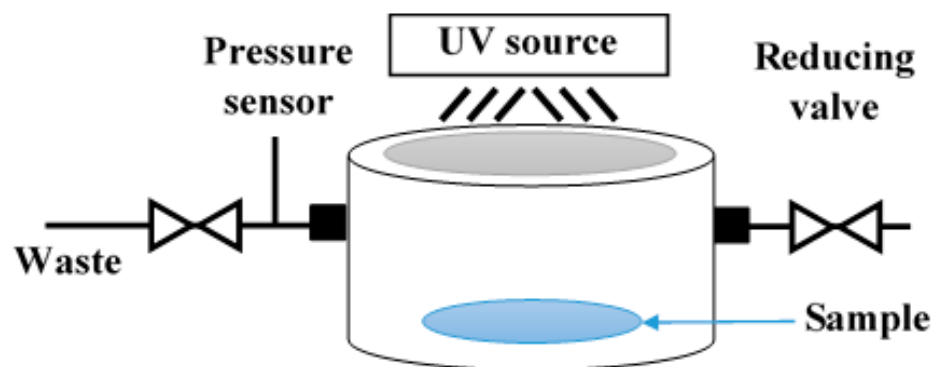
Figure 6. Scheme of the photo-reactor used to decompose N_2O gas.

In addition, to highlight the significance of the present study for potential industrial application, the degradation of SMX is performed in the secondary effluent of municipal wastewater treatment plants collected in Clermont-Ferrand, France. Prior to being used as a wastewater matrix, it is filtered through a 0.45 μm PTFE membrane and further analyzed by total organic analysis (Shimadzu, TOC-L) and ionic chromatography (Thermo Scientific, ICS 5000). The data are presented in Table 1.

Table 1. Concentration of inorganic ions and inorganic and organic carbon.

Species	Concentration (mg L^{-1})
Cl^-	100
NO_3^-	59
SO_4^{2-}	53
PO_4^{3-}	<LOD [1]
Na^+	131
NH_4^+	4
K^+	40
Mg^{2+}	9
Ca^{2+}	25
Inorganic C	47
Organic C	7

[1] Under the Limit of Detection.

The identification of SMX transformation by-products is obtained by ultra-high performance liquid chromatography (UHPLC) coupled with high-resolution mass spectrometry (HRMS) performed on an Orbitrap Q-Exactive (Thermo scientific). The column is a Phenomenex Kinetex C18 (1.7 μm × 100 Å; 100 × 2.1 mm) and the temperature is set at 30 °C. The initial gradient is 5% ACN and 95% water acidified with 1% formic acid, followed by a linear gradient to 99% ACN within 8.5 min and kept constant during 1 min. The flow rate is 0.45 mL min^{-1} and the injection volume is 5 μL. Ionization is set to 3.2 kV (ESI+) and 3.0 kV (ESI−).

4. Conclusions

The preparation of different TiO_2 nanostructures including nanotube layers and thin films has been performed using electrochemical anodization and the sol–gel method,

respectively. Their performance in versatile photocatalytic applications has been assessed by investigating their ability to degrade gaseous and aqueous pollutants under UVA light, i.e., N_2O and sulfamethoxazole. The best samples in both the photocatalytic reactions are those showing a nanotubular morphology (F20 and F40), probably due to their high specific surface area and excellent charge carriers transport, compared to others samples (F0, F60, F80 and SG) that show non-ordered and less porous nanostructures. In addition, the degradation mechanism of sulfamethoxazole has been proposed and has highlighted the crucial role of hydroxyl radicals. This study is significant since it proves the photocatalytic versatility of anodic TiO_2 nanotube layers in different applications such as the remediation of air and water. Indeed, the degradation of sulfamethoxazole has been tested in secondary effluents from a wastewater treatment plant and has confirmed the efficiency of the anodic TiO_2 nanotube layers.

References

1. Hashimoto, K.; Irie, H.; Fujishima, A. TiO_2 Photocatalysis: A Historical Overview and Future Prospects. *Jpn. J. Appl. Phys. Part 1 Regul. Pap. Short Notes Rev. Pap.* **2005**, *44*, 8269–8285. [CrossRef]
2. Schneider, J.; Matsuoka, M.; Takeuchi, M.; Zhang, J.; Horiuchi, Y.; Anpo, M.; Bahnemann, A.; Schneider, D.W. Understanding TiO_2 Photocatalysis Mechanisms and Materials. *Chem. Rev.* **2014**, *114*, 9919–9986. [CrossRef] [PubMed]
3. Moradeeya, P.G.; Sharma, A.; Kumar, M.A.; Basha, S. Titanium Dioxide Based Nanocomposites—Current Trends and Emerging Strategies for the Photocatalytic Degradation of Ruinous Environmental Pollutants. *Environ. Res.* **2022**, *204*, 112384. [CrossRef] [PubMed]
4. Wu, M.J.; Bak, T.; O'Doherty, P.J.; Moffitt, M.C.; Nowotny, J.; Bailey, T.D.; Kersaitis, C. Photocatalysis of Titanium Dioxide for Water Disinfection: Challenges and Future Perspectives. *Int. J. Photochem.* **2014**, *2014*, 973484. [CrossRef]

5.   Kumar, S.G.; Devi, L.G. Review on Modified TiO_2 Photocatalysis under UV/Visible Light: Selected Results and Related Mechanisms on Interfacial Charge Carrier Transfer Dynamics. *J. Phys. Chem. A* **2011**, *115*, 13211–13241. [CrossRef] [PubMed]

6.   Lan, Y.; Lu, Y.; Ren, Z. Mini Review on Photocatalysis of Titanium Dioxide Nanoparticles and Their Solar Applications. *Nano Energy* **2013**, *2*, 1031–1045. [CrossRef]

7.   Motola, M.; Dworniczek, E.; Satrapinskyy, L.; Chodaczek, G.; Grzesiak, J.; Gregor, M.; Plecenik, T.; Nowicka, J.; Plesch, G. UV Light-Induced Photocatalytic, Antimicrobial, and Antibiofilm Performance of Anodic TiO_2 Nanotube Layers Prepared on Titanium Mesh and Ti Sputtered on Silicon. *Chem. Pap.* **2019**, *73*, 1163–1172. [CrossRef]

8.   Yemmireddy, V.K.; Hung, Y.C. Using Photocatalyst Metal Oxides as Antimicrobial Surface Coatings to Ensure Food Safety—Opportunities and Challenges. *Compr. Rev. Food Sci. Food Saf.* **2017**, *16*, 617–631. [CrossRef]

9.   Fagan, R.; McCormack, D.E.; Dionysiou, D.D.; Pillai, S.C. A Review of Solar and Visible Light Active TiO2 Photocatalysis for Treating Bacteria, Cyanotoxins and Contaminants of Emerging Concern. *Mater. Sci. Semicond. Process.* **2016**, *42*, 2–14. [CrossRef]

10.   Motola, M.; Zazpe, R.; Hromadko, L.; Prikryl, J.; Cicmancova, V.; Rodriguez-Pereira, J.; Sopha, H.; Macak, J.M. Anodic TiO_2 Nanotube Walls Reconstructed: Inner Wall Replaced by ALD TiO_2 Coating. *Appl. Surf. Sci.* **2021**, *549*, 149306. [CrossRef]

11.   Macak, J.M.; Zlamal, M.; Krysa, J.; Schmuki, P. Self-Organized TiO_2 Nanotube Layers as Highly Efficient Photocatalysts. *Small* **2007**, *3*, 300–304. [CrossRef]

12.   Kubacka, A.; Diez, M.S.; Rojo, D.; Bargiela, R.; Ciordia, S.; Zapico, I.; Albar, J.P.; Barbas, C.; Martins Dos Santos, V.A.P.; Fernández-García, M.; et al. Understanding the Antimicrobial Mechanism of TiO_2-Based Nanocomposite Films in a Pathogenic Bacterium. *Sci. Rep.* **2014**, *4*, 4134. [CrossRef]

13.   Macák, J.M.; Tsuchiya, H.; Ghicov, A.; Schmuki, P. Dye-Sensitized Anodic TiO_2 Nanotubes. *Electrochem. Commun.* **2005**, *7*, 1133–1137. [CrossRef]

14.   Regonini, D.; Chen, G.; Leach, C.; Clemens, F.J. Comparison of Photoelectrochemical Properties of TiO_2 Nanotubes and Sol-Gel. *Electrochim. Acta* **2016**, *213*, 31–36. [CrossRef]

15.   Beranek, R.; Tsuchiya, H.; Sugishima, T.; Macak, J.M.; Taveira, L.; Fujimoto, S.; Kisch, H.; Schmuki, P. Enhancement and Limits of the Photoelectrochemical Response from Anodic TiO_2 Nanotubes. *Appl. Phys. Lett.* **2005**, *87*, 243114. [CrossRef]

16.   Thompson, T.L.; Yates, J.T. Surface Science Studies of the Photoactivation of TIO2—New Photochemical Processes. *Chem. Rev.* **2006**, *106*, 4428–4453. [CrossRef]

17.   Lee, K.; Mazare, A.; Schmuki, P. One-Dimensional Titanium Dioxide Nanomaterials: Nanotubes. *Chem. Rev.* **2014**, *114*, 9385–9454. [CrossRef]

18.   Roy, P.; Berger, S.; Schmuki, P. TiO_2 Nanotubes: Synthesis and Applications. *Angew. Chem.—Int. Ed.* **2011**, *50*, 2904–2939. [CrossRef]

19.   Sopha, H.; Baudys, M.; Krbal, M.; Zazpe, R.; Prikryl, J.; Krysa, J.; Macak, J.M. Scaling up Anodic TiO_2 Nanotube Layers for Gas Phase Photocatalysis. *Electrochem. Commun.* **2018**, *97*, 91–95. [CrossRef]

20.   Hanif, M.B.; Sihor, M.; Liapun, V.; Makarov, H.; Monfort, O.; Motola, M. Porous vs. Nanotubular Anodic TiO_2: Does the Morphology Really Matters for the Photodegradation of Caffeine? *Coatings* **2022**, *12*, 1002. [CrossRef]

21.   Crini, G.; Lichtfouse, E. Advantages and Disadvantages of Techniques Used for Wastewater Treatment. *Environ. Chem. Lett.* **2019**, *17*, 145–155. [CrossRef]

22.   Devipriya, S.; Yesodharan, S. Photocatalytic Degradation of Pesticide Contaminants in Water. *Sol. Energy Mater. Sol. Cells* **2005**, *86*, 309–348. [CrossRef]

23.   Wilkinson, J.L.; Boxall, A.B.A.; Kolpin, D.W.; Leung, K.M.Y.; Lai, R.W.S.; Wong, D.; Ntchantcho, R.; Pizarro, J.; Mart, J.; Echeverr, S.; et al. Pharmaceutical Pollution of the World's Rivers. *Proc. Natl. Acad. Sci. USA* **2022**, *119*, e2113947119. [CrossRef] [PubMed]

24.   Mackuľak, T.; Černanský, S.; Fehér, M.; Birošová, L.; Gál, M. Pharmaceuticals, Drugs, and Resistant Microorganisms—Environmental Impact on Population Health. *Curr. Opin. Environ. Sci. Health* **2019**, *9*, 40–48. [CrossRef]

25.   Decision 2020/1161/EU Commission Implementing Decision (EU) 2020/1161-4 August 2020. Establishing a Watch List of Substances for Union-Wide Monitoring in the Field of Water Policy Pursuant to Directive 2008/105/EC of the European Parliament and of the Council. *Off. J. Eur. Union* **2020**, *257*, 32–35.

26.   Ebitani, K.; Morokuma, M.; Kim, J.H.; Morikawa, A. Photocatalytic Decomposition of Nitrous Oxide on Cu Ion-Containing ZSM-5 Catalyst. *J. Catal.* **1993**, *141*, 725–728. [CrossRef]

27.   deRichter, R.; Caillol, S. Fighting Global Warming: The Potential of Photocatalysis against CO_2, CH_4, N_2O, CFCs, Tropospheric O_3, BC and Other Major Contributors to Climate Change. *J. Photochem. Photobiol. C Photochem. Rev.* **2011**, *12*, 1–19. [CrossRef]

28.   Sano, T.; Negishi, N.; Mas, D.; Takeuchi, K. Photocatalytic Decomposition of N_2O on Highly Dispersed Ag+ Ions on TiO_2 Prepared by Photodeposition. *J. Catal.* **2000**, *194*, 71–79. [CrossRef]

29.   Obalová, L.; Reli, M.; Lang, J.; Matějka, V.; Kukutschová, J.; Lacný, Z.; Kočí, K. Photocatalytic Decomposition of Nitrous Oxide Using TiO_2 and Ag-TiO_2 Nanocomposite Thin Films. *Catal. Today* **2013**, *209*, 170–175. [CrossRef]

30.   Kočí, K.; Krejčíková, S.; Šolcová, O.; Obalová, L. Photocatalytic Decomposition of N_2O on Ag-TiO_2. *Catal. Today* **2012**, *191*, 134–137. [CrossRef]

31.   Matějová, L.; Polách, L.; Lang, J.; Šihor, M.; Reli, M.; Brunátová, T.; Daniš, S.; Peikertová, P.; Troppová, I.; Kočí, K. Novel TiO_2 Prepared from Titanyl Sulphate by Using Pressurized Water Processing and Its Photocatalytic Activity Evaluation. *Mater. Res. Bull.* **2017**, *95*, 30–46. [CrossRef]

32. Kočí, K.; Reli, M.; Troppová, I.; Šihor, M.; Kupková, J.; Kustrowski, P.; Praus, P. Photocatalytic Decomposition of N_2O over TiO_2/g-C_3N_4 Photocatalysts Heterojunction. *Appl. Surf. Sci.* **2017**, *396*, 1685–1695. [CrossRef]

33. Yuan, R.; Wang, M.; Liao, L.; Hu, W.; Liu, Z.; Liu, Z.; Guo, L.; Li, K.; Cui, Y.; Lin, F.; et al. 100% N2O Inhibition in Photocatalytic NOx Reduction by Carbon Particles over Bi_2WO_6/TiO_2 Z-Scheme Heterojunctions. *Chem. Eng. J.* **2023**, *453*, 139892. [CrossRef]

34. Sihor, M.; Hanif, M.B.; Thirunavukkarasu, G.K.; Liapun, V.; Edelmannova, M.F.; Roch, T.; Satrapinskyy, L.; Pleceník, T.; Rauf, S.; Hensel, K.; et al. Anodization of Large Area Ti: A Versatile Material for Caffeine Photodegradation and Hydrogen Production. *Catal. Sci. Technol.* **2022**, *12*, 5045–5052. [CrossRef]

35. Monfort, O.; Roch, T.; Gregor, M.; Satrapinskyy, L.; Raptis, D.; Lianos, P.; Plesch, G. Photooxidative Properties of Various BiVO4/TiO2 Layered Composite Films and Study of Their Photocatalytic Mechanism in Pollutant Degradation. *J. Environ. Chem. Eng.* **2017**, *5*, 5143–5149. [CrossRef]

36. Ao, X.; Liu, W.; Sun, W.; Yang, C.; Lu, Z.; Li, C. Mechanisms and Toxicity Evaluation of the Degradation of Sulfamethoxazole by MPUV/PMS Process. *Chemosphere* **2018**, *212*, 365–375. [CrossRef]